THE JOURNAL OF PHYSICAL CHEMISTRY A
A JOURNAL OF THE AMERICAN CHEMICAL SOCIETY

pubs.acs.org/JPCA

Article

# Photophysical Exploration of Two Isomers of Octaethyltrioxopyrrocorphin

Sayantan Bhattacharya, Dustin E. Nevonen, Alexander J. Auty, Arthur Graf, Martin Appleby, Nivedita Chaudhri, Dimitri Chekulaev, Christian Brückner,* Adrien A. P. Chauvet,* and Victor N. Nemykin*

Cite This: J. Phys. Chem. A 2023, 127, 7694−7706

Read Online

ACCESS | Metrics & More | Article Recommendations | Supporting Information

**ABSTRACT:** The introduction of three β-oxosubstituents to octaethylporphyrin by means of an oxidation/rearrangement reaction generates the trioxopyrrocorphin chromophore. Pyrrocorphins (hexahydroporphyrins) are generally nonaromatic, but we recently demonstrated trioxopyrrocorphins to possess considerable aromatic character. This contribution explores the photophysical characteristics of these unusual chromophores. In agreement with density functional theory modeling, the UV−vis and magnetic circular dichroism spectra of the two—out of the four possible—triketone regioisomers investigated conform to the Gouterman model of porphyrinoid optical spectra, in alignment with their aromaticity. Their excited-state dynamics shed further light on the degree to which β-oxo substitutions tune the photophysical properties of porphyrinoids. Introduction of β-oxo functionalities increases the rate and yield of intersystem crossing and shortens the triplet state lifetime. Unexpectedly, the singlet oxygen generation yield of both pyrrocorphins remains relatively high, with modes of distortion from planarity likely enhancing triplet energy transfer. This work thus expands our understanding of a rare class of porphyrinoids and further characterizes them as sustaining aromatic porphyrinic π-systems. Our findings suggest triple β-oxo substitution as a viable route toward the development of novel, high-singlet oxygen yield porphyrinic photosensitizers.

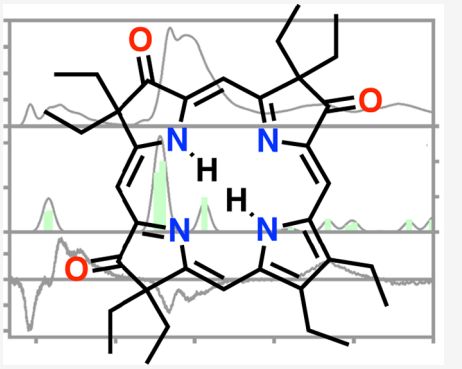


## 1. INTRODUCTION

Porphyrinic chromophores have high and tunable absorption cross-sections in the visible spectral range. They are thus key to the development of, for instance, novel photocatalytic and light-harvesting materials. Finding effective ways to fine-tune porphyrins is therefore essential.

The chromophores of porphyrins are characterized by the presence of a Hückel-aromatic 18 π-electron system, cross-conjugated with two additional double bonds. This arrangement is typically described as the porphyrinic 18 + 4 π-system (Figure 1). Sequential reactions that convert one, or both, of the cross-conjugated β,β′-double bonds to single bonds generate dihydro- and tetrahydroporphyrins, respectively, of the chlorin, bacteriochlorin, or isobacteriochlorin classes.[1−6] The resulting 18 + 4, 18 + 2, or 18 π-electron systems of the (hydro)porphyrin chromophores are the origin of their characteristic electronic properties, as well as their broad utility as, e.g., dyes, sensors, redox noninnocent metal chelators, or photosensitizers.[7,8] The removal of an additional double bond from the tetrahydroporphyrins typically results in the interruption of the aromatic 18 π-electron system. The hexahydroporphyrin chromophore may either be in its pyrrocorphin form (2,3,7,8,12,13-hexahydroporphyrin) or in its tautomeric porphyrinogen (5,10,15,20,22,24-hexahydroporphyrin) leuco form (not shown).[6] Classic studies have suggested that the free base hexahydroporphyrins exist preferentially in the porphyrinogen tautomeric form, while their nickel(II) complexes prefer the pyrrocorphin form.[9−15]

Studies of synthetic β-alkylpyrrocorphins, such as **1Ni**, by Battersby and coworkers,[16] Smith and Simpson,[17] or Lahiri and Stolzenberg,[10] were inspired by the pioneering work by Eschenmoser and coworkers who recognized pyrrocorphins as intermediates in the biosynthesis of vitamin $B_{12}$ (Figure 2).[9,11−15]

More recently, examples of pyrrocorphins or pyrrocorphin analogues of the *meso*-tetrakis(pentafluorophenyl)porphyrin series emerged.[10,18−21] For instance, triple-cycloaddition formed pyrrocorphins **2**/**2Ni**;[19] reduction of a bacteriochlorin-type bisadduct also realized a pyrrocorphin.[21] The electronic properties of the pyrrocorphins received only minimal attention.

Received: May 14, 2023
Revised: August 18, 2023
Published: September 10, 2023

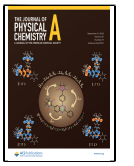







https://doi.org/10.1021/acs.jpca.3c03184
J. Phys. Chem. A 2023, 127, 7694−7706

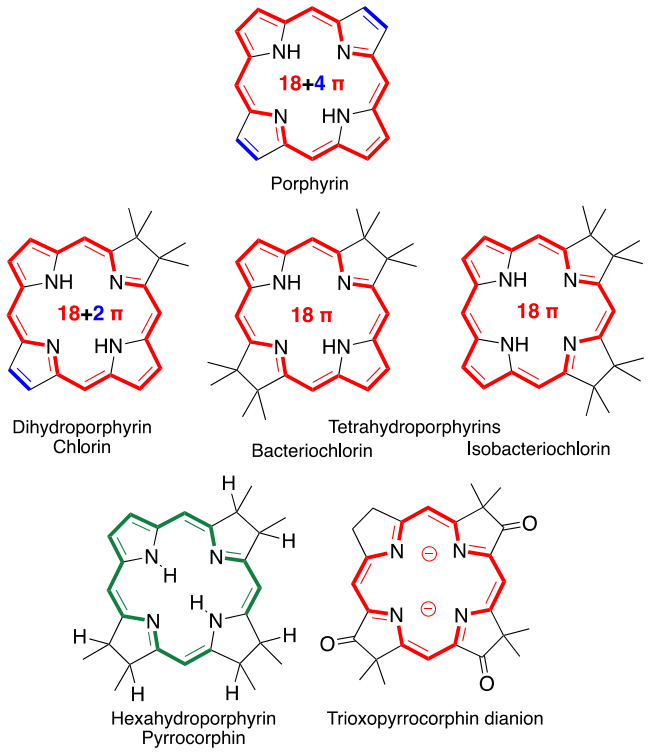


**Figure 1.** Framework structures of the hydroporphyrin classes are indicated. Aromatic $\pi$-systems are highlighted in red, and cross-conjugated double bonds are in blue. Conjugated but nonmacrocycle-aromatic $\pi$-systems are in green.

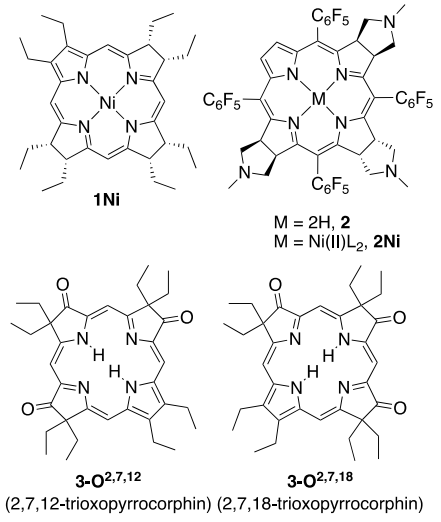


**Figure 2.** Framework structures of the hydroporphyrins indicated.

An alternative way to modify the porphyrinic cross-conjugated double bonds is to introduce $\beta$-oxo-functionalities into $\beta$-alkylporphyrins. One simple method is their treatment with hydrogen peroxide when dissolved in concentrated sulfuric acid.[22−27] This classic, 90-year-old reaction,[22] when applied to octaethylporphyrin (**OEP**), generates one $\beta$-oxochlorin, five isomers of the corresponding $\beta,\beta'$-dioxochromophores, as well as two out of the four possible $\beta,\beta',\beta''$-trioxopyrrocorphins (**3-O$^{2,7,12}$** and **3-O$^{2,7,18}$**), in addition to other products.[23−29] The chemical, coordination, and physical properties of $\beta$-oxochlorin have long been investigated.[27,30−47] More recently, the chemistry and photophysical properties of the dioxo-derivatives were the subject of several studies, revealing the large impact of the $\beta$-oxo-substituents on the electronic properties of the porphyrinic chromophore.[45,47−54] Remarkable regiochemical influences were revealed in porphyrinic chromophores carrying multiple $\beta$-oxo-substituents,[28,47,53,55,56] including the *meso*-arylporphodilactones.[57−60]

Among the $\beta$-oxoporphyrinoids, the triketones stand out as the least studied compound class. The nickel and copper complexes of the isomeric trioxopyrrocorphins **3-O$^{2,7,12}$** or **3-O$^{2,7,18}$** were prepared, and their structure, axial binding properties, and electrochemical properties were studied.[48,49,61,62] We recently described the preparation of the hitherto unknown regioisomers of the triketones and revealed their unique electronic properties.[29,47] They are, against expectations for regular pyrrocorphins, aromatic, with the regioisomers varying significantly in their degree of aromaticity. As a reduction of one or two oxo-groups led to a degradation of the aromaticity, the aromatic nature of the trioxopyrrocorphins could be unambiguously linked to the presence of the $\beta$-oxo-substituents.[47]

We previously investigated the electronic effects of one and two $\beta$-oxo-substitutions on the benchmark compound **OEP**; we showed that the effects of $\beta$-oxosubstitution were additive, with, for example, a two-fold increase in the intersystem crossing (ISC) rate per substitution.[56] This effect was correlated to the increase in spin−orbit coupling due to the out-of-plane vibration of the extra carbonyl group.

The present work explores the spectroscopic properties of triply-oxosubstituted octaethylporphyrinoids.[29] Along with their steady-state absorption, emission, and magnetic circular dichroism (MCD) spectra, we present their excited-state dynamics using transient UV−vis and transient IR spectroscopy of the two most readily accessible pyrrocorphin triketone isomers **3-O$^{2,7,12}$** and **3-O$^{2,7,18}$**. The spectral properties are correlated with density functional theory (DFT) and time-dependent-DFT (TDDFT) calculations of their electronic structures. This work thus furthers the understanding of the tuning effects of the auxochrome $\beta$-oxo functionalities, in general, and of the electronic properties of $\beta$-trioxopyrrocorphins, in particular. The findings are expected to be generalizable beyond **OEP**-derived $\beta$-oxoporphyrins.

## 2. EXPERIMENTAL SECTION

**2.1. Materials.** The two $\beta,\beta',\beta''$-trioxopyrrocorphin isomers **3-O$^{2,7,12}$** and **3-O$^{2,7,18}$** were prepared by oxidation of **OEP** according to our recent report.[29]

**2.2. Photophysical Methods.** *2.2.1. Steady-State UV−Vis and Fluorescence Spectroscopy.* Steady-state UV−vis and fluorescence measurements (including excitation-emission spectra) were performed in $CH_2Cl_2$ on a Carry 60 UV−vis spectrometer and a FluroMax spectrophotometer, respectively. Fluorescence quantum yields were determined relative to that of *meso*-tetraphenylporphyrin.[63]

*2.2.2. Emission Lifetime and Transient UV−Vis Absorption Spectroscopy.* All samples were degassed using multiple freeze-pump-thaw cycles before measurements. Samples were held in 2 mm path-length quartz cells and were continuously stirred during experiments using a magnetic stirring system. Emission lifetime has been measured using Mini-Tau lifetime spectrometer (Edinburgh Instruments). Femtosecond to nanosecond transient absorption (TA) spectroscopy has


https://doi.org/10.1021/acs.jpca.3c03184
J. Phys. Chem. A 2023, 127, 7694−7706

been performed in a commercial TA spectrometer (Helios, Ultrafast Systems) in the Lord Porter Ultrafast Laser Laboratory, Sheffield. Nanosecond to millisecond TA spectroscopy has been performed in a home-built setup in the same location. Details of the methods were reported earlier.[56] A full description of the methods has been provided in the Supporting Information.

*2.2.3. Singlet Oxygen Quantum Yields.* The quantum yield of singlet oxygen production, $\phi_{1O2}$, by $\beta$-trioxopyrrocorphins in acetonitrile solution was measured directly by detecting the emission from photo-generated singlet oxygen at 1275 nm. The $\phi_{1O2}$ value was determined relative to a standard, perinaphthenone ($\phi_{1O2}$ = 100%).[64] Details of the method have been provided in the Supporting Information.

*2.2.4. Time-Resolved IR (TRIR) Spectroscopy.* TRIR was performed at the Lord Porter Ultrafast Laser Spectroscopy Laboratory, University of Sheffield. A Ti:Sapphire regenerative amplifier (Spitfire ACE PA-40, Spectra-Physics) provided 800 nm pulses (40 fs FWHM, 10 kHz, 1.2 mJ). 400 nm pulses for sample excitation were generated through frequency doubling of a portion of the amplifier fundamental. The broadband mid-IR probe pulse, centered at 1700 $cm^{-1}$, was produced by an automated commercially available optical parametric amplifier equipped with a difference frequency mixing stage (TOPAS, Light Conversion), seeded by a portion of the amplifier fundamental. Further details have been provided in the Supporting Information.

*2.2.5. MCD Spectroscopy.* MCD data were obtained using a Jasco V-1500 spectropolarimeter (1.5 T electromagnet). Two spectra were recorded for each sample, one using a parallel field and the other using an antiparallel field. Spectral intensities were expressed as molar ellipticity per T.[65−67]

*2.2.6. Computations.* All DFT and TDDFT calculations were performed using the Gaussian 09 software.[68] The starting geometries for all compounds, computed as their octamethyl derivatives **X′**, were optimized using B3LYP;[69] then M06[70] was used for the DFT and TDDFT calculations. For geometry optimizations and TDDFT calculations, a 6-311G(d) basis set was used for all atoms. In calculations of the relative energies of the tautomeric forms, a larger 6-311+G(d,p) basis set was used for all atoms. The solvent effects were modeled using the Polarizable Continuum Model (PCM) approach[71] using $CH_2Cl_2$ as a solvent.[72] The equilibrium geometries were confirmed with the frequency calculations and, more specifically, by the absence of imaginary frequencies. The QMForge[73] program was used to compile molecular orbital contributions from the single-point calculations.

## 3. RESULTS AND DISCUSSION

**3.1. Steady-State Absorption and Emission Properties.** The steady-state absorption and emission spectra of the two $\beta,\beta',\beta''$-trioxopyrrocorphin isomers **3-O$^{2,7,12}$** and **3-O$^{2,7,18}$** are typical for aromatic porphyrinic chromophores, with a strong Soret band and a structured Q-band region, but also showing differences between the two isomers (Figure 3); the spectra conform to previous reports and are reiterated here for context.[26,27,29]

In comparison with its isomer, the spectrum of **3-O$^{2,7,12}$** is generally less defined, has lower absorptivity, has a more blue-shifted longest wavelength of absorption ($\lambda_{max}$), and has a much larger intensity ratio between the Soret band and the longest wavelength Q-band ($\lambda_{max}$). It was also found to carry

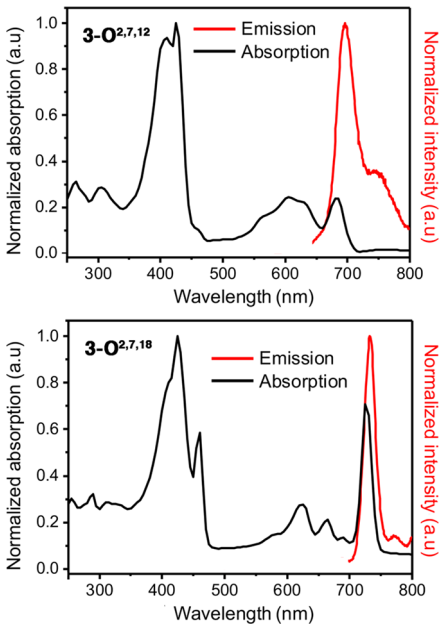


**Figure 3.** Normalized absorption and emission spectra ($CH_2Cl_2$, room temperature) of the trioxopyrrocorphin isomers are indicated. Excitation emission spectra are provided as Supporting Information (Figure S-1).

a smaller diatropic ring current, as shown by the smaller spread between the diatropic shifts of the $^1$H NMR signals of the inner NH and peripheral $\beta$-H atoms; in other words, **3-O$^{2,7,12}$** is less aromatic than **3-O$^{2,7,18}$**.[29] The correlation between the relative position of $\lambda_{max}$ and the degree of aromaticity confirms a previous assessment by Zhang, Sessler, and coworkers.[74]

Both trioxo-compounds are emissive, with the small Stoke's shift characteristic of other aromatic tetrapyrroles:[29] the fluorescence quantum yield $\phi_f$ of **3-O$^{2,7,12}$** is 0.15, that of **3-O$^{2,7,18}$** is 0.08 (the photophysical data are summarized in Table 1). The emission yield of the "less aromatic" isomer **3O$^{2,7,12}$** is higher, and the emission bands are broader than the sharp emission of isomer **3O$^{2,7,18}$**.[29]

**3.2. Emission Lifetimes.** Emission kinetics of the two trioxopyrrocorphin isomers **3-O$^{2,7,12}$** and **3-O$^{2,7,18}$** were determined using time-correlated single photon counting (TCSPC) measurements (Figure 4). The emissions decay monoexponentially with lifetimes of 3.4 ± 0.1 and 2.7 ± 0.2 ns for **3-O$^{2,7,12}$** and **3-O$^{2,7,18}$**, respectively. Following the cascaded electronic relaxation scheme of free base porphyrins, chlorins, and dioxochlorins,[56,75,76] these decay times can be attributed to the singlet lifetime of $S_1(Q_x)$. We previously found the emission lifetimes to decrease by half with each oxo-substitution, from 11 ns for the parent **OEP**, to 5.5 ns for the monooxochlorin, to 1.5−3.3 ns for the dioxochlorins.[56] The emission lifetime for the triketones thus remains similar to those observed for the dioxochlorin isomers. Accordingly, we observe a limit on the tuning of the emission lifetime by means of the number of $\beta$-oxosubstituents introduced into the chromophore.

From these lifetimes, we computed the radiative and nonradiative rates for both isomers using $k_r = \phi_f/\tau_S$ and $\sum k_{nr} = (1 - \phi_f)/\tau_S$, where $\phi_f$ is the experimentally determined fluorescence quantum yield and $\tau_S$ is the singlet lifetime; the values for $\phi_f$, $\tau_S$, and $\sum k_{nr}$ are listed in Table 1.


https://doi.org/10.1021/acs.jpca.3c03184
J. Phys. Chem. A 2023, 127, 7694−7706

Table 1. Photophysical Data (in Degassed $CH_2Cl_2$) of the Two Trioxopyrrocorphin Isomers Indicated

| sample | Soret bands (nm) | Q-bands (nm) | $\tau_S$ (ns) | $\phi_f$[a] | $\phi_{ISC}$[b] | $k_r$ ($s^{-1}$) | $\sum k_{nr}$ ($s^{-1}$)[c] | $k_{ISC}$ ($s^{-1}$)[d] | $\phi_{1O2}$[e] |
|---|---|---|---|---|---|---|---|---|---|
| 3-$O^{2,7,12}$ | 405, 425, 465 | 565, 605, 634, 685 | 3.42 ± 0.01 | 0.15 | 0.46 | $4.5 \times 10^7$ | $2.5 \times 10^8$ | $1.7 \times 10^8$ | 0.58 ± 0.16 |
| 3-$O^{2,7,18}$ | 425, 459 | 580, 625, 665, 689, 725 | 2.67 ± 0.02 | 0.08 | 0.92 | $3.2 \times 10^7$ | $3.4 \times 10^8$ | $2.7 \times 10^8$ | 0.59 ± 0.09 |

[a]Fluorescence quantum yield has been calculated by reference against *meso*-tetraphenylporphyrin ($\phi_f$ s 0.13 in $CH_2Cl_2$).[34] Errors are ±5% for $\phi_f$. [b]To measure the yield of $S_1 \rightarrow T_n$ intersystem crossing, we compared the bleach amplitude of the ground-state absorption bands due to $T_n$ at the asymptote of the $S_1$ decay with the bleach amplitude due to $S_1$ immediately after the excitation. Probe wavelength has been chosen where there is negligible absorption in $S_1 \rightarrow S_n$ and $T_1 \rightarrow T_n$. Errors are ±12% for $\phi_{ISC}$. [c]$\sum k_{nr} = (1 - \phi_f)/\tau_S$. [d]$k_{ISC} = \phi_{ISC}/\tau_S$. [e]Singlet oxygen quantum yield was measured by direct detection of the emission from photo-generated $^1O_2$ at 1275 nm.

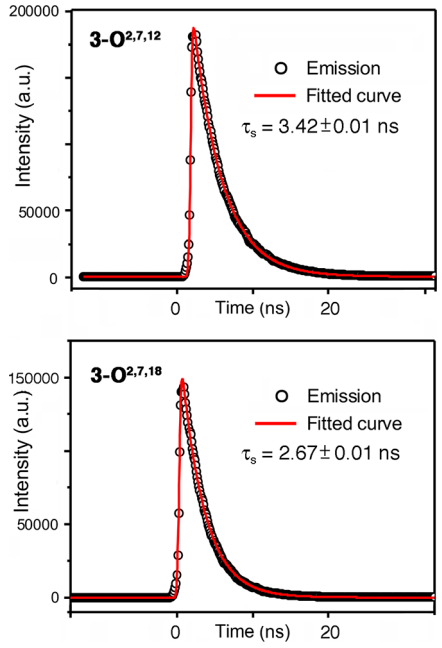


**Figure 4.** Time-correlated single photon counting (TCSPC) measurements of the emission spectra (degassed $CH_2Cl_2$) of the trioxopyrrocorphin isomers are indicated; $\lambda_{excitation}$ = 400 nm.

**3.3. MCD Spectra.** The major spectroscopic features in the UV−vis and MCD spectra of triketones 3-$O^{2,7,12}$ and 3-$O^{2,7,18}$ resemble those in the spectra of porphyrins, their *β*-oxo-derivatives, and other porphyrinoid analogues (Figure 5A).[28,77−82] Consequently, we will use porphyrin-related assignments in the description of the spectra.

In case of 3-$O^{2,7,12}$, the lowest energy band at 683 nm was assigned to correspond to a $Q_x$ transition. This band is associated with the MCD B-term of negative amplitude at 685 nm. Three overlapping bands at 630, 606, and 562 nm are associated with three MCD B-terms observed at 631, 604, and 563 nm. The most intense band at 606 nm, associated with the lowest energy MCD B-term of positive amplitude, was assigned as the $Q_y$ transition. A $Q_x$−$Q_y$ splitting energy of 0.24 eV follows from this assignment. The UV−vis spectrum of 3-$O^{2,7,12}$ is dominated by two bands in the Soret region, at 426 and 409 nm. These bands are associated with MCD B-terms of negative amplitude at 427 and 406 nm.

The lowest energy band in 3-$O^{2,7,18}$ is at 727 nm, significantly red-shifted compared to the corresponding band observed for the 3-$O^{2,7,12}$ isomer. This band is associated with an MCD B-term of negative amplitude at 724 nm; it was assigned as the $Q_x$ transition. Four UV−vis bands at 688, 664, 623, and 585 nm are associated with MCD B-terms at 693, 659, 624, and 583 nm. Again, the lowest energy MCD B-term with a positive amplitude at 624 nm was assigned to the $Q_y$ transition. The energy difference between $Q_x$ and $Q_y$ bands in 3-$O^{2,7,18}$ is 0.27 eV, i.e., 13% larger than that observed for the 3-$O^{2,7,12}$ isomer. In the Soret band region of the optical spectrum of the 3-$O^{2,7,18}$ isomer, three bands at 458, 425, and 407 are the most prominent. They are associated with two MCD B-terms of negative amplitude, observed at 462 and 428 nm. No clear MCD signal is associated with the band at 407 nm.

According to the perimeter model that proved to be very useful for the interpretation of the MCD spectra of a wide variety of porphyrinoids,[83−88] the negative-to-positive sequences (in ascending energy) for the $Q_x$ and $Q_y$ transitions in 3-$O^{2,7,12}$ and 3-$O^{2,7,18}$ are indicative of a ΔHOMO > ΔLUMO relationship when using the classic Gouterman's four-orbital description (whereby ΔHOMO is the energy difference between Gouterman's $a_{1u}$ and $a_{2u}$ occupied orbitals and ΔLUMO is the energy difference between Gouterman's $e_{g(x)}$ and $e_{g(y)}$ pair of unoccupied orbitals in the standard $D_{4h}$ point group notation).[7,89] As will be shown below, DFT calculations correlate well with this interpretation.

**3.4. Computations.** To better rationalize the photo- and magnetophysical properties observed for triketones 3-$O^{2,7,12}$ and 3-$O^{2,7,18}$, we conducted DFT calculations on all possible tautomers (Table 2).

It is well known that the choice of exchange-correlation functional can affect the calculated relative energies of the tautomers;[90−97] we use the M06 functional known to provide low errors (typically within 1.5−2.0 kcal/mol) for the computed thermochemical data for a large variety of organic compounds. The expected tautomer with two NH protons located on the opposite five-membered rings (one pyrrolic and one oxopyrrolic ring) has the lowest energy. The other three theoretically possible NH tautomers (tautomers 2−4) possess ∼5.3−7.3 kcal/mol higher energies. This essentially eliminates their presence in the ambient temperature solution equilibrium mixture. The NH−NH tautomers 1−4 can also be transformed into NH−OH tautomers O1−O3, but their energies are even significantly higher than those of NH−NH tautomers.

Interestingly, the DFT-predicted energy diagram for the lowest energy tautomers of 3-$O^{2,7,12}$ and 3-$O^{2,7,18}$ (Figure 6) and the frontier orbitals for these two isomers (Figure 7) resemble those in the parent **OEP**.[28]

In particular, the HOMO and HOMO-1 resemble classic Gouterman's $a_{1u}$ and $a_{2u}$ orbitals, respectively, while the LUMO and LUMO+1 resemble the pair of Gouterman's $e_g$ orbitals (in a standard $D_{4h}$ point group notation). The DFT-predicted energy gap between LUMO and LUMO+1 in 3-$O^{2,7,12}$ is significantly smaller compared to the corresponding gap in 3-$O^{2,7,18}$ isomer. More importantly, with agreement to the MCD spectra discussed above, the DFT predicts a ΔHOMO > ΔLUMO relationship for the frontier orbitals for


https://doi.org/10.1021/acs.jpca.3c03184
J. Phys. Chem. A 2023, 127, 7694−7706

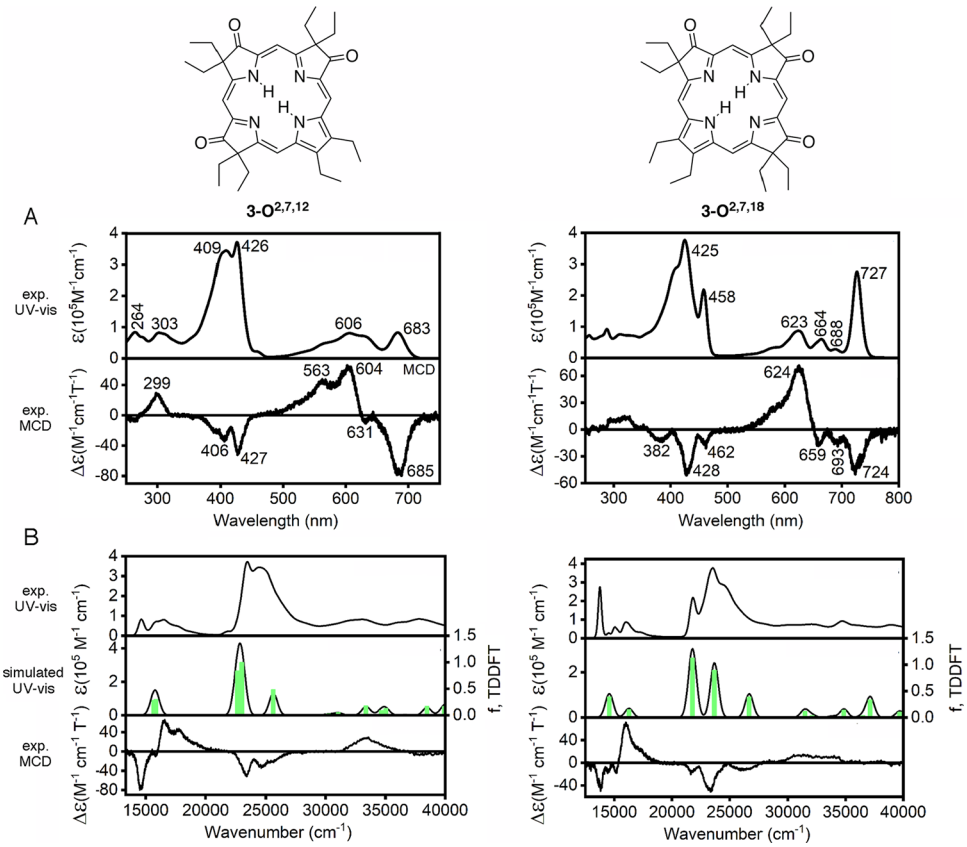


**Figure 5.** (A) Experimental UV−vis and MCD spectra of the pyrrocorphin triketones are indicated (all in $CH_2Cl_2$) and plotted against wavelength. (B) Experimental UV−vis, TDDFT-predicted UV−vis, and experimental MCD spectra of the pyrrocorphin triketones are indicated and plotted against wavenumber.

**Table 2. Relative Energies of All Possible Tautomers of 3-O$^{2,7,12}$ and 3-O$^{2,7,18}$ Compounds Predicted by DFT Calculations (M06 Functional)**

| | relative energies, kcal/mol | |
|---|---|---|
| tautomer[a] | 3-O$^{2,7,12}$ | 3-O$^{2,7,18}$ |
| 1 | 0 | 0 |
| 2 | 6.59 | 6.02 |
| 3 | 5.33 | 6.65 |
| 4 | 7.34 | 6.97 |
| O1 | 33.57 | 31.44 |
| O2 | 34.39 | 33.01 |
| O3 | 33.51 | 31.94 |

[a]Tautomer 1: NH on pyrrolic and NH on opposite $\beta$-oxopyrrolic rings; tautomers 2 and 3: NH on pyrrolic and on NH adjacent $\beta$-oxopyrrolic rings; tautomer 4: two NH on opposite $\beta$-oxopyrrolic rings; tautomer O1: NH on pyrrolic and OH on opposite $\beta$-oxopyrrolic rings (this transforms it from NH C=O to N and C−OH); tautomers O2 and O3: NH on pyrrolic and OH on the adjacent oxo functionality (this transforms it from NH C=O to N and C−OH). A graphical representation of all the tautomers considered is presented in the Supporting Information.

3-O$^{2,7,12}$ and 3-O$^{2,7,18}$, as also shown by the MCD measurement.

TDDFT calculations on triketone isomers 3-O$^{2,7,12}$ and 3-O$^{2,7,18}$ were conducted to reveal the nature of the excited states and possibly align the major transitions with Gouterman's four-orbital theory. In general, the TDDFT-predicted spectra correlate well with the experimental data (Figure 5B).

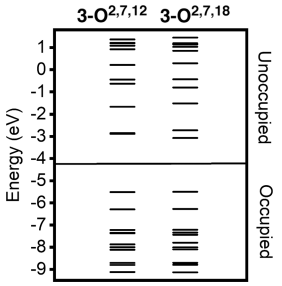


**Figure 6.** DFT-predicted energy-level diagrams for the two trioxopyrrocorphins are indicated.

In case of the 3-O$^{2,7,18}$ isomer, TDDFT predicted that the $Q_x$ (at 686 nm) band is dominated (~90%) by a HOMO → LUMO single-electron transition (Tables 3 and 4), while the $Q_y$ band (predicted at 614 nm) is dominated by a HOMO → LUMO+1 single-electron transition. TDDFT-predicted energy separation between $Q_x$ and $Q_y$ bands (0.24 eV) correlate well with the experimentally observed value (0.27 eV); their predicted energies are within 0.1 eV to the experiment.

TDDFT predicts two major transitions for the 3-O$^{2,7,18}$ isomer in the Soret band region. The lower energy transition (at 459 nm) correlates well with the 450 nm band observed experimentally and is dominated by a HOMO-1 → LUMO single-electron excitation. The second transition, predicted at 422 nm, matches the experimentally observed band at 425 nm, and is dominated by the HOMO-1 → LUMO+1 single-electron excitation band.


https://doi.org/10.1021/acs.jpca.3c03184
J. Phys. Chem. A 2023, 127, 7694−7706

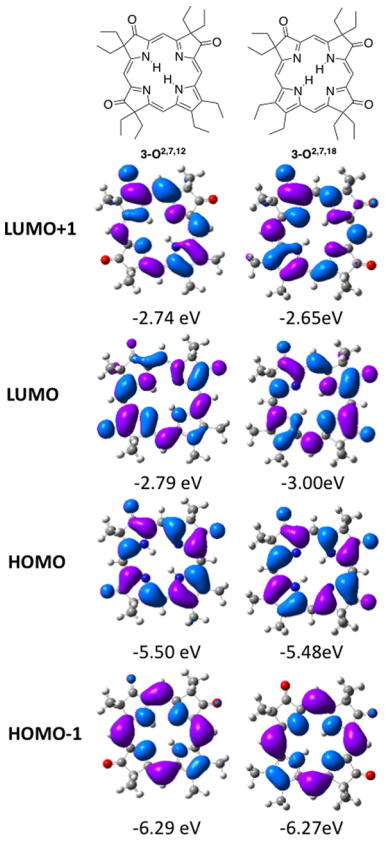


**Figure 7.** DFT-predicted frontier MOs for the trioxopyrrocorphins indicated. For details, see Supporting Information.

**Table 3. Selected TDDFT-Predicted Excited States of 3-O$^{2,7,12}$ Using the M06/6-311G(d) Method**

| excited state | wavelength (nm) | energy (eV) | oscillator strength, f | % contributions |
|---|---|---|---|---|
| 1 | 637 | 1.946 | 0.2824 | H → L + 1 (82%), H-1 → L (13%), H → L (4%) |
| 2 | 630 | 1.967 | 0.2979 | H → L (87%), H-1 → L + 1 (9%), H → L + 1 (4%) |
| 3 | 442 | 2.806 | 0.8432 | H-1 → L (69%), H → L + 1 (12%), H-1 → L + 1 (10%), H → L + 2 (8%) |
| 4 | 435 | 2.851 | 0.9979 | H-1 → L + 1 (74%), H-1 → Λ (13%), H → L (8%), H → L + 2 (3%), H → L + 1 (2%) |
| 6 | 390 | 3.178 | 0.4879 | H → L + 2 (88%), H-1 → L + 1 (6%), H-1 → L (4%) |
| 15 | 300 | 4.136 | 0.1784 | H → L + 3 (97%) |
| 19 | 285 | 4.344 | 0.1333 | H-6 → L (37%), H → L + 4 (24%), H-6 → L + 1 (20%), H-7 → L (11%), H-7 → L + 1 (6%) |
| 25 | 260 | 4.771 | 0.1743 | H-1 → L + 3 (94%) |
| 28 | 250 | 4.950 | 0.1677 | H-1 → L + 4 (56%), H → L + 5 (36%) |
| 29 | 248 | 5.008 | 0.1346 | H → L + 5 (46%), H-1 → L + 4 (39%), H-4 → L + 2 (8%) |

Similarly, TDDFT predicts that the Q-band region in the **3-O$^{2,7,12}$** isomer is dominated by HOMO → LUMO and HOMO → LUMO+1 single-electron excitations, while the Soret band region is dominantly HOMO-1 → LUMO and HOMO-1 → LUMO+1 single-electron excitations. The TDDFT-predicted $Q_x$−$Q_y$ energy splitting is significantly underestimated (~0.02 eV), but still within the typical error for TDDFT methods. Thus, TDDFT predicts that the major transitions in **3-O$^{2,7,12}$** and **3-O$^{2,7,18}$** isomers can be described using Gouterman's four-orbital model.[7,89] This is another indication of the presence of the (unexpected) aromatic system in these pyrrocorphin triketones.[29]

**Table 4. Selected TDDFT-Predicted Excited States of 3-O$^{2,7,18}$ Using the M06/6-311G(d) Method**

| excited state | wavelength (nm) | energy (eV) | oscillator strength, f | % contributions |
|---|---|---|---|---|
| 1 | 686 | 1.807 | 0.3910 | H → L (91%), H-1 → L + 1 (7%) |
| 2 | 614 | 2.019 | 0.1481 | H → L + 1 (75%), H-1 → L (22%), H → L (2%) |
| 3 | 459 | 2.700 | 1.1300 | H-1 → L (74%), H → L + 1 (23%), H → L + 2 (3%) |
| 5 | 422 | 2.936 | 0.8982 | H-1 → L + 1 (90%), H → L (8%) |
| 7 | 375 | 3.309 | 0.3891 | H → L + 2 (94%), H-1 → L (2%) |
| 13 | 318 | 3.904 | 0.1187 | H → L + 3 (78%), H-1 → L + 2 (15%), H-7 → L (2%) |
| 19 | 287 | 4.321 | 0.1402 | H → L + 4 (76%), H-6 → L (9%), H-7 → L (6%), H-1 → L + 3 (3%), H-6 → L + 1 (3%) |
| 23 | 269 | 4.604 | 0.3379 | H-1 → Λ + 3 (81%), H-6 → L + 1 (7%), H-7 → L (4%), H → L + 5 (3%), H → L + 4 (3%) |
| 27 | 252 | 4.920 | 0.1060 | H-1 → L + 4 (63%), H → L + 5 (32%) |
| 29 | 244 | 5.072 | 0.1555 | H → L + 5 (59%), H-1 → L + 4 (32%), H-7 → L + 1 (2%) |

**3.5. Transient Absorption Spectroscopy.** TA spectra have been collected on degassed solutions of trioxopyrrocorphin isomers **3-O$^{2,7,18}$** (Figure 8) and **3-O$^{2,7,12}$** (Figure 9) in the fs to ms regime.

For both compounds, TA spectra consist of the ground-state bleach (GSB) peaks superimposed on the broad positive excited-state absorption (ESA) bands. The TA signals of both isomers show similar features to those of the octaalkyl-*β*,*β*′-dioxochlorins studied previously.[56] In case of triketone **3-O$^{2,7,18}$**, singular value decomposition (SVD) of the fs−ns kinetics (Figure 8b,c) reveals time constants of 2.4 ± 0.1 ns and a nondecaying component, which coincide with the 2.6 ± 0.1 ns and 66 ± 1 *μ*s components extracted from the ns−ms probe kinetics (Figure 8e,f). In accordance with the TCSPC results, the ns-component is attributed to the $S_1$ fluorescence lifetime. The 66 *μ*s-component is attributed to the lowest triplet state lifetime. When comparing the decay-associated spectra (DAS) derived from SVD, the discrepancy in relative amplitude between the two DAS in Figure 8c,f is most probably an artifact of the analysis: the 2.6 ns DAS (Figure 8f) is too close to the ~1.5 ns instrument response function. One can, however, appreciate the agreement between the derived DAS spectral features between the fs−ns and the ns−ms experiments.

In case of triketone **3-O$^{2,7,12}$**, the fitting of the fs−ns probe kinetics in Figure 9b revealed time constants of 4.2 ± 0.1 ns as well as a longer-living component, both of which coincide with the 4.3 ± 0.2 ns and 68 ± 3 *μ*s monitored in the ns−ms probe kinetics (Figure 9e). In accordance with the TCSPC results for the **3-O$^{2,7,18}$** isomer, the ~4 ns-component is attributed to the $S_1$ emission lifetime. The 68 *μ*s-component is thus attributed to the triplet state lifetime.



https://doi.org/10.1021/acs.jpca.3c03184
J. Phys. Chem. A 2023, 127, 7694−7706

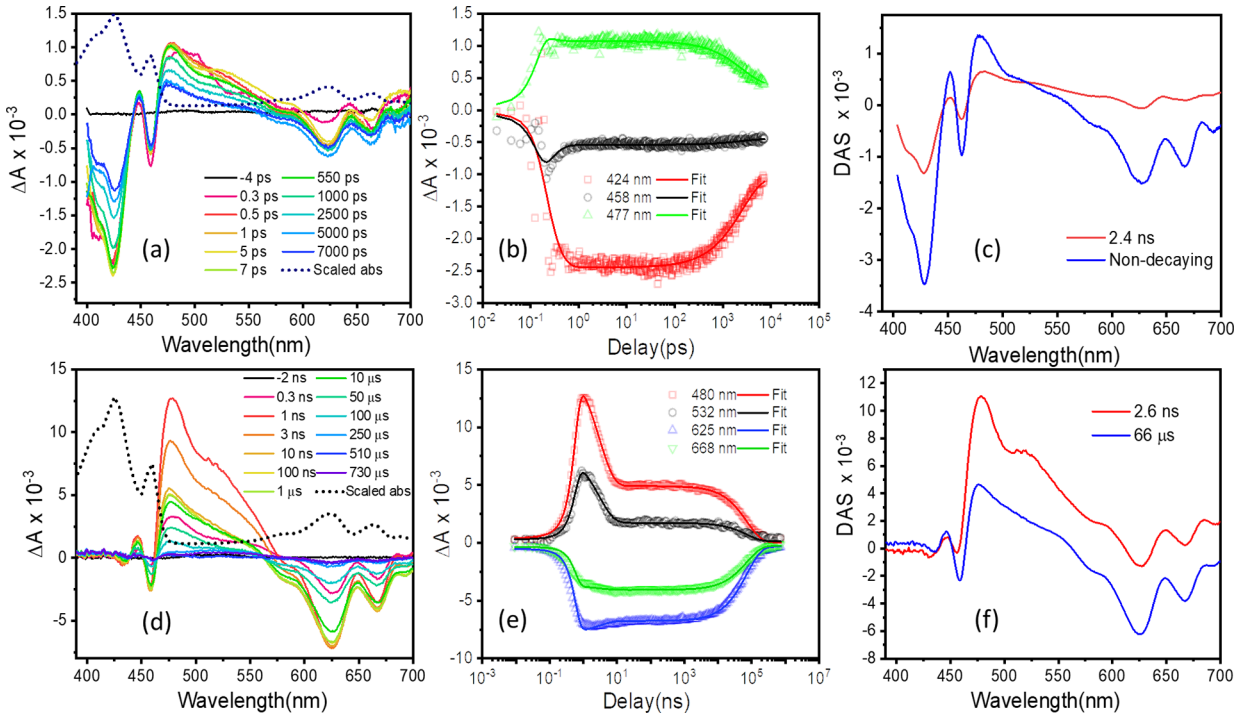


**Figure 8.** Transient absorption spectra recorded for triketone **3-O**[2,7,18]: (a) fs−ns and (d) ns−ms regimes, along with full probe kinetics in the (b) fs−ns and (e) ns−ms regimes. The decay-associated spectra (DAS) calculated from singular value decomposition (SVD) are shown for both the fs−ns (c) and ns−ms (f) experiments. Note that the "non-decaying" component in (c), which corresponds to the 66 $\mu$s DAS in (f), is labeled as such because it cannot be resolved within the fs−ns delay range. Also note that the spectral window in the ns−ms experiments was restricted to >430 nm. See Supporting Information for experimental and fitting details.

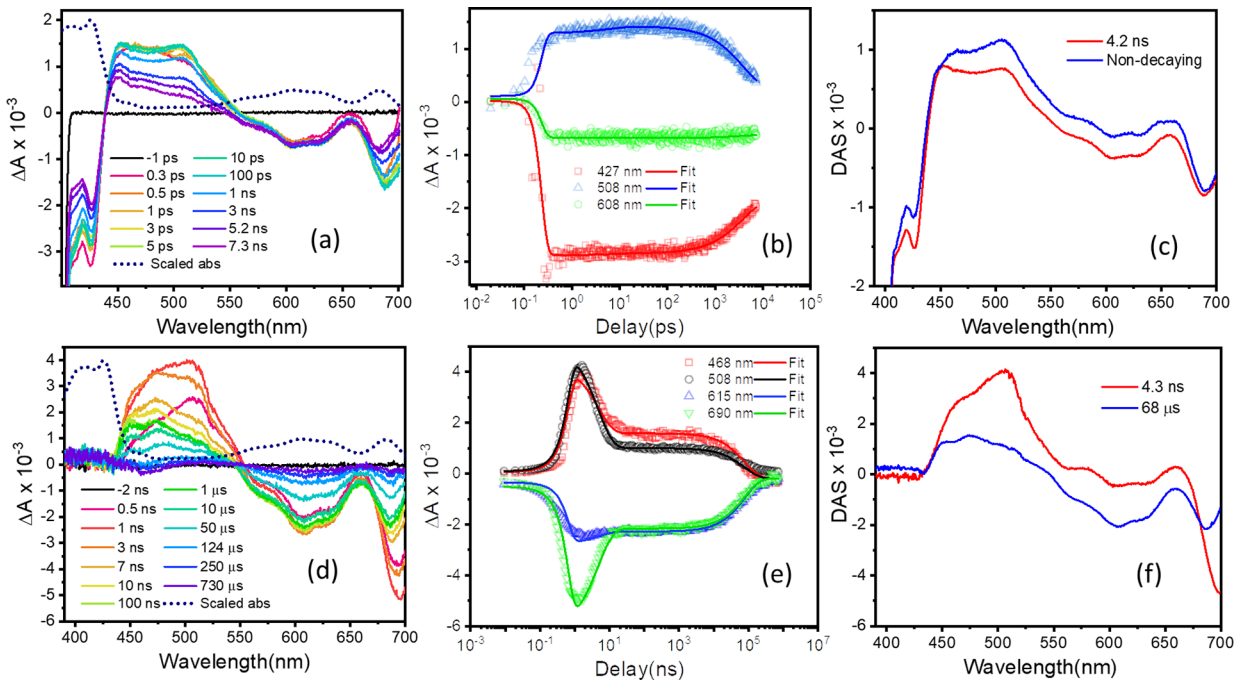


**Figure 9.** Transient absorption spectra recorded for triketone **3-O**[2,7,12]: (a) fs−ns and (d) ns−ms regimes along with full probe kinetics in the (b) fs−ns and (e) ns−ms regimes. The decay-associated spectra (DAS) calculated from singular value decomposition (SVD) are shown for both the fs−ns (c) and ns−ms (f) experiments. Note that the "non-decaying" component in (c), which corresponds to the 66 $\mu$s DAS in (f), is labeled as such because it cannot be resolved within the fs−ns delay range. Also note that the spectral window in the ns−ms experiments was restricted to >430 nm. See Supporting Information for experimental and fitting details.

The negative feature at 685 nm for triketone **3-O**[2,7,12] (Figure 9a) shows a redshift within picoseconds and a subsequent blueshift over the remaining time window. This shift of the transient bleach signal, which was not captured by the SVD analysis, is representative of vibrational cooling via solvent coupling. Similar shifts were previously monitored for



https://doi.org/10.1021/acs.jpca.3c03184
J. Phys. Chem. A 2023, 127, 7694−7706

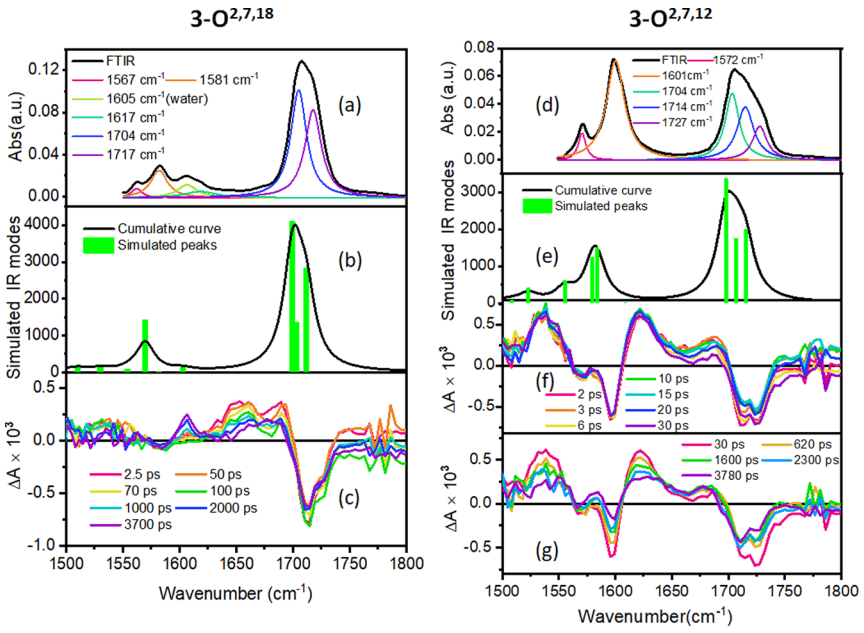


**Figure 10.** Experimental solution state ($CH_2Cl_2$) FTIR (a, d) and DFT-predicted IR modes of the pyrrocorphin triketones indicated (b, e), all on an energy scale. TA spectra from time-resolved IR measurements at representative time delays following excitation with a 400-nm excitation pulse (c, f, g); arrows indicate the direction in which the spectra evolved. For experimental details, see Supporting Information. Both the compounds have been kept under vacuum for a few hours to minimize the effect of water absorption at 1606 $cm^{-1}$. FTIR spectra of **3-O$^{2,7,18}$** and **3-O$^{2,7,12}$** have been measured after exposure to different degrees of vacuum, showing that the high vacuum condition is suitable to remove most of the adsorbed water (Figure S-2 in the Supporting Information).

OEP, chlorin, and dioxochlorins.[56] It is also interesting to note that the negative spectral feature around 600 nm in Figure 6a, which appears "instantaneously" (i.e., during the excitation pulse duration), does not evolve in the ps range. The stability of this signal suggests that the singlet and triplet states have similar spectral shapes and strengths in this region.

The ISC rates, $k_{ISC}$, for each chromophore were computed using the experimental $S_1$ lifetimes as well as the ISC quantum yields ($\phi_{ISC}$) calculated from the ns−ms TA data (Table 1). We compute $k_{ISC}$ rates of $1.7 \times 10^8$ and $2.7 \times 10^8$ $s^{-1}$ for **3-O$^{2,7,12}$** and **3-O$^{2,7,18}$**, respectively. This represents a 3.5-fold and near 6-fold increase, respectively, when compared to the $k_{ISC}$ rate of $4.75 \times 10^7$ $s^{-1}$ of the parent **OEP**.[56] The triplet lifetime in both trioxopyrrocorphin isomers is similarly reduced to 65−70 $\mu$s, as was also predicted in our earlier studies of the dioxochromophores.[56] Indeed, we have shown that the carbonyl out-of-plane vibration of the $\beta$-oxo substituents causes the $T_n - S_0$ energy difference to decrease and the corresponding spin−orbit coupling matrix elements to increase. Accordingly, we expect crossings between the $T_n$ and $S_0$ potential energy surfaces at high carbonyl vibrational angles, leading to a decrease in triplet state lifetimes in the trioxo-substituted chromophores.

**3.6. Singlet Oxygen Quantum Yields.** The quantum yield of singlet oxygen production ($\phi_{1O2}$) by both $\beta$-trioxopyrrocorphin isomers **3-O$^{2,7,12}$** and **3-O$^{2,7,18}$** (in acetonitrile) was measured directly by detection of the emission from photo-generated singlet oxygen, at 1275 nm. We determined $\phi_{1O2}$ to be high and essentially identical for both isomers, at ~0.6 (0.58 ± 0.16 and 0.59 ± 0.09, respectively). Generally, the singlet oxygen quantum yield depends on the efficiency of the ISC ($\phi_{ISC}$), the triplet lifetime, and the efficiency of the energy transfer from triplet state of a photosensitizer to ground-state oxygen.[98,99] Both compounds possess similar triplet lifetimes (68 $\mu$s and 66 $\mu$s, respectively). However, the triketone **3-O$^{2,7,12}$** has a $\phi_{ISC}$ yield ($\phi_{ISC}$ = 0.46) that is about half that of **3-O$^{2,7,18}$** ($\phi_{ISC}$ = 0.98). Hence, to compensate for this $\phi_{ISC}$ disparity, the energy transfer efficiency, from triplet state to triplet oxygen, of **3-O$^{2,7,12}$** must be twice that of **3-O$^{2,7,18}$**. In other words, the energy transfer efficiency for **3-O$^{2,7,12}$** must be near-unity.

Conformational effects may rationalize the differences in energy transfer efficiencies between the two isomers. Indeed, distortions from planar structures have been pointed out as an essential factor for the triplet energy transfer to oxygen: while the porphyrin $T_1$ vibrational ground-state energy is close to the energy needed for the excitation of ground to singlet state oxygen, the electron spin exchange mechanism is most efficient if the energy discrepancy is minimized (ideally, resonance condition) by out-of-plane distortions.[100] We thus suspect the macrocycle excited-state conformation of **3-O$^{2,7,12}$** to be more distorted than that of **3-O$^{2,7,18}$**. Alternatively, the higher yield for the energy transfer process from the chromophore triplet state to ground-state oxygen could also be due to excited-state aromaticity reversal.[101,102] If such was the case, we would expect a stark modification of the C=C stretch vibrational mode, while in the excited state. However, our transient IR measurements were not conclusive on this matter (see below).

**3.7. Steady-State and Transient FTIR Spectra.** As expected of macrocycles bearing multiple $\beta$-carbonyl groups, their solution state-steady state fourier-transform infrared (FTIR) spectra display multiple, overlapping absorption bands in the region between 1500 and 1850 $cm^{-1}$ (Figure 10a,d and Table 5). To aid in their assignment, a Lorentzian decomposition into the underlying vibrational bands was


https://doi.org/10.1021/acs.jpca.3c03184
J. Phys. Chem. A 2023, 127, 7694−7706

**Table 5. Transient FTIR Data of the Trioxopyrrocorphin Isomers Indicated**

| sample | ground-state bleaches ($cm^{-1}$) | initial ESA band ($cm^{-1}$) (lifetimes) | ESA bands at 3800 ps ($cm^{-1}$) |
|---|---|---|---|
| 3-$O^{2,7,18}$ | 1584, 1712 | 1535 (2.6 ns), 1657 (2.6 ns), 1690 (2.6 ns) | 1606, 1677 |
| 3-$O^{2,7,12}$ | 1571, 1598, 1711 | 1533 (78 ns), 1685 (78 ns), 1539 (4.3 ns), 1625 (4.3 ns), 1688 (4.3 ns) | 1550, 1584, 1630, 1667 |

applied. DFT calculations have also been performed, and the experimental Lorentzian fitted peaks can be matched to the DFT-based oscillator frequencies (Figure 10b,e and Table 5).

DFT modeling predicts C=C stretching modes near ~1584 and ~1569 $cm^{-1}$ for **3-O$^{2,7,12}$** and **3-O$^{2,7,18}$**, respectively. In the case of **3-O$^{2,7,12}$**, the peak at 1697 $cm^{-1}$ is assigned to single carbonyl stretching, whereas the 1706 and 1714 $cm^{-1}$ peaks correspond to in-plane out-of-phase and in-phase C=O stretching modes, accordingly (see Supporting Information Figure S-3a−c). Similar modes for **3-O$^{2,7,18}$** have been predicted at 1698, 1702, and 1711 $cm^{-1}$ (see Figure S-4a−c).

Following excitation at 400 nm, the TRIR absorption spectrum of **3-O$^{2,7,18}$** is characterized by bleach signals at 1584 and 1712 $cm^{-1}$, which coincide with the ground-state IR absorption bands at 1581 and 1704/1717 $cm^{-1}$, respectively (Figure 10c). These bleach signals sit on top of ESA bands with distinct features at 1535, 1657, and 1690 $cm^{-1}$. The latter bleach and ESA signals decay concomitantly with the rise of new ESA bands at 1606 and 1677 $cm^{-1}$ with a time constant of 2.6 ns (see Supporting Information Figure S-5). These growing ESA features are thus ascribed to the formation of the triplet state.

The corresponding TRIR spectra of isomer **3-O$^{2,7,12}$** show similar bleaching signals corresponding to ground-state absorption bands at 1572, 1601, 1712, and 1727 $cm^{-1}$. Prominent ESA bands are present at 1533 and 1625 $cm^{-1}$. The presence of ESA bands that are about equal in amplitude to the bleach signals indicates a clear restructuring of the macrocycle conjugated $\pi$-system while in the excited state. Because these large ESA bands are present at both early and later times, they are characteristics of both the singlet and triplet state of the molecule. In comparison with **3-O$^{2,7,18}$**, the TRIR signals of **3-O$^{2,7,12}$** are marked by more intense and more distinct ESA features, which could be ascribed to a more distorted excited state. In turn, a more distorted conformation would help explain the near unity energy transfer from the molecule's triplet state to singlet oxygen previously discussed. However, to draw a direct correlation between the shape of the IR spectra and the molecule's planarity requires further modeling of the molecule's excited state.

It is also possible to estimate the triplet yield using the present TRIR data. The partial recovery of the GSB at ~1710 $cm^{-1}$ in the ns regime directly reflects the proportion of singlet excited-state molecules returning to the ground state, while the remaining GSB signal is ascribed to the triplet states. Thus, assuming that both singlet and triplet states have similar extinction coefficient in this spectral region (see Supporting Information for details), we computed a triplet yield of ~0.82 for **3-O$^{2,7,18}$** and ~ 0.43 for **3-O$^{2,7,12}$**. These data are in good agreement with the previous ISC yields calculated from TA experiments (i.e., 0.98 and 0.46, respectively).

## 4. CONCLUSIONS

The ground and excited-state photophysical properties of two positional isomers of the octaethyltrioxopyrrocorphins, **3-O$^{2,7,12}$** and **3-O$^{2,7,18}$**, were probed experimentally using UV−vis, MCD, fluorescence spectroscopies, and time-resolved optical and FTIR measurements. Their interpretation was supported using DFT and TDDFT approaches.

The data presented suggest that the electronic structure of **3-O$^{2,7,12}$** and **3-O$^{2,7,18}$** isomers resemble, on a qualitative level, the electronic structure of the parent **OEP**. Correspondingly, the UV−vis spectra of the two pyrrocorphin triketones can be rationalized on the basis of Gouterman's four-orbital model and are reflective of HOMO/HOMO-1 → LUMO/LUMO +1 single-electron excitations, with a ΔHOMO > ΔLUMO relationship for **3-O$^{2,7,12}$** and **3O$^{2,7,18}$**. Also, the excited-state properties are comparable to those of the aromatic diketone analogues. The ISC rates are 1.7 and 2.7 × $10^8$ $s^{-1}$ for **3-O$^{2,7,12}$** and **3O$^{2,7,18}$**, respectively, and the triplet state lifetime is about 70 $\mu$s for both triketones. On the one hand, the sum of this (partially known)[29,103] body of evidence further cements the view that these triketones sustain aromatic, porphyrin-like $\pi$-systems, even though a nonaromatic pyrrocorphin-like macrocycle $\pi$-structure could have been expected. On the other hand, the similarities between the excited-state dynamics of the tri- and di-ketones imply that the limit of the ability to tune the porphyrinic chromophore of OEP by means of $\beta$-oxo substituents was reached at the disubstitution level. However, while a third $\beta$-oxo substitution does not affect the excited-state dynamics beyond those observed for the diketones, it seems to play a key role in the ability of the triketones to generate singlet oxygen. The singlet oxygen yield of both triketones remains high, about 60%. The additional $\beta$-oxo substitution results in a more pronounced static or dynamic deviation from planarity, which might enhance the process. The present study thus reinforces the influence of $\beta$-oxo substitution and calls for further investigation of this class of molecules as photosensitizers.

## ■ ASSOCIATED CONTENT

### Supporting Information

The Supporting Information is available free of charge at https://pubs.acs.org/doi/10.1021/acs.jpca.3c03184.

Extended experimental descriptions; excitation spectra; FTIR spectra under different vacuum conditions; individual DFT vibrational modes in .gif format; global multiexponential fittings of the TRIR kinetics; and details of the estimation of the triplet quantum yields from the TRIR data (PDF)

## ■ AUTHOR INFORMATION

### Corresponding Authors

**Christian Brückner** − *Department of Chemistry, University of Connecticut, Storrs, Connecticut 06269-3060, United States;* orcid.org/0000-0002-1560-7345; Email: c.bruckner@uconn.edu



https://doi.org/10.1021/acs.jpca.3c03184
J. Phys. Chem. A 2023, 127, 7694−7706

**Adrien A. P. Chauvet** − *Department of Chemistry, University of Sheffield, Sheffield S3 7HF, U.K.*; orcid.org/0000-0002-1649-0898; Email: a.chauvet@sheffield.ac.uk

**Victor N. Nemykin** − *Department of Chemistry, University of Tennessee, Knoxville, Tennessee 37996-1600, United States*; orcid.org/0000-0003-4345-0848; Email: vnemykin@utk.edu

### Authors

**Sayantan Bhattacharya** − *Department of Chemistry, University of Sheffield, Sheffield S3 7HF, U.K.*; Present Address: Imperial College London, Department of Life Sciences, London, U.K

**Dustin E. Nevonen** − *Department of Chemistry, University of Tennessee, Knoxville, Tennessee 37996-1600, United States*

**Alexander J. Auty** − *Department of Chemistry, University of Sheffield, Sheffield S3 7HF, U.K.*

**Arthur Graf** − *Department of Chemistry, University of Sheffield, Sheffield S3 7HF, U.K.*

**Martin Appleby** − *Department of Chemistry, University of Sheffield, Sheffield S3 7HF, U.K.*

**Nivedita Chaudhri** − *Department of Chemistry, University of Connecticut, Storrs, Connecticut 06269-3060, United States*; orcid.org/0000-0001-9604-606X

**Dimitri Chekulaev** − *Department of Chemistry, University of Sheffield, Sheffield S3 7HF, U.K.*

Complete contact information is available at: https://pubs.acs.org/10.1021/acs.jpca.3c03184

### Author Contributions

S.B. measured and analyzed the steady-state absorption, emission spectra, emission kinetics, fs−ns TA, ns−ms TA data. M.A., D.C., A.J.A., and S.B. developed the bespoke setup, measured, and analyzed TRIR data. A.G. and M.A. recorded singlet oxygen data. D.E.N. recorded the MCD spectra and V.N.N. performed the computations. N.C. performed the syntheses of the compounds studied. S.B., A.A.P.C., and V.N.N. devised and executed the study. C.B., A.A.P.C., S.B., and V.N.N. collaborated in the writing of the manuscript with input from all authors.

### Notes

The authors declare no competing financial interest.

## ■ ACKNOWLEDGMENTS

This work was supported by the US National Science Foundation under Grant Numbers CHE-1800361 (to C.B.) and 2153081 (V.N.N.). Support from WestGrid and the University of Tennessee to V.N.N. is also greatly appreciated. S.B. and A.A.P.C. acknowledge the support from EPSRC through Grants: EP/R045305/1 and EP/R042802/1. We thank Julia Weinstein, The University of Sheffield, for the TRIR measurements. We also thank Chi-Kwong (Chris) Chang, Michigan State University, for a donation of the OEP used to prepare the triketones used in this study.

## ■ ABBREVIATIONS

DAS: decay-associated spectra
DFT: density functional theory
ESA: excited-state absorption
FTIR: Fourier-transform infrared
GSB: ground-state bleach
HOMO: highest occupied molecular orbital
ISC: intersystem crossing
LUMO: lowest unoccupied molecular orbital
MCD: magnetic circular dichroism
OEP: octaethylporphyrin
SVD: singular value decomposition
TCSPC: time correlated single photon counting
TDDFT: time-dependent density functional theory
TRIR: time-resolved infrared
UV−vis: ultraviolet and visible

## ■ REFERENCES

(1) Montforts, F.-P.; Gerlach, B.; Höper, F. Discovery and Synthesis of Less Common Natural Hydroporphyrins. *Chem. Rev.* **1994**, *94*, 327−347.
(2) Brückner, C.; Samankumara, L.; Ogikubo, J.: Syntheses of Bacteriochlorins and Isobacteriochlorins. In *Handbook of Porphyrin Science*; Kadish, K. M., Smith, K. M., Guilard, R., Eds.; World Scientific: River Edge, NY, 2012; Vol. *17*, pp 1−112.
(3) Taniguchi, M.; Lindsey, J. S. Synthetic Chlorins, Possible Surrogates for Chlorophylls, Prepared by Derivatization of Porphyrins. *Chem. Rev.* **2017**, *117*, 344−535.
(4) Liu, Y.; Zhang, S.; Lindsey, J. S. Total Synthesis Campaigns toward Chlorophylls and Related Natural Hydroporphyrins − Diverse Macrocycles Unrealized Opportunities. *Nat. Prod. Rep.* **2018**, *35*, 879−901.
(5) Borbas, K. E. In *Handbook of Porphyrin Science*; World Scientific: River Edge, NY, 2016; Vol. *36*, pp 1−149.
(6) Jux, N.; Montforts, F.-P.; Haake, E. In *Science of Synthesis Knowledge Updates*; Georg Thieme Verlag KG: Stuttgart, Germany, 2022; pp 111−141.
(7) Gouterman, M. In *The Porphyrins*; Dolphin, D., Ed.; Academic Press: New York, NY: 1978; Vol. *3*, pp 1−165.
(8) Battersby, A. R. Tetrapyrroles: The Pigments of Life. *Nat. Prod. Rep.* **2000**, *17*, 507−526.
(9) Johansen, J. E.; Piermattie, V.; Angst, C.; Diener, E.; Kratky, C.; Eschenmoser, A. Interconversion of the Chromophore Systems of Porphyrinogen and 2,3,7,8,12,13-Hexahydroporphyrin. *Angew. Chem., Int. Ed. Engl.* **1981**, *20*, 261−263.
(10) Lahiri, G. K.; Stolzenberg, A. M. Reductive Chemistry of Nickel Hydroporphyrins. 3. Facile Preparation of Hexahydroporphyrin Complexes by Reduction of (Octaethylisobacteriochlorin)-Nickel(II). *Angew. Chem., Int. Ed. Engl.* **1993**, *32*, 429−432.
(11) Waditschatka, R.; Kratky, C.; Jaun, B.; Heinzer, J.; Eschenmoser, A. Chemistry of Pyrrocorphins: Structure of Nickel-(II) CCCCC-Octaethylpyrrocorphinate in the Solid State and in Solution. Observation of the Inversion Barrier between Enantiomorphically Ruffled Conformers. *J. Chem. Soc., Chem. Commun.* **1985**, 1604−1607.
(12) Waditschatka, R.; Eschenmoser, A. Chemistry of Pyrrocorphins: Stereoselectivity During Porphyrinogen - Pyrrocorphin Tautomerism. *Angew. Chem.* **1983**, *95*, 639−640.
(13) Waditschatka, R.; Diener, E.; Eschenmoser, A. Chemistry of Pyrrocorphins: Carbon Methylation of Pyrrocorphinates on the Ligand Periphery. *Angew. Chem.* **1983**, *95*, 641−642.
(14) Eschenmoser, A. Chemistry of Corphinoids. *Ann. N. Y. Acad. Sci.* **1986**, *471*, 108−129.
(15) Summers, J. S.; Stolzenberg, A. M. The *cis*-Influence of Hydroporphyrin Macrocycles on the Axial Ligation Equilibria of Co(II) and Zn(II) Porphyrin Complexes. *J. Am. Chem. Soc.* **1993**, *115*, 10559−10567.
(16) De Voss, J. J.; Leeper, F. J.; Battersby, A. R. Synthetic Studies Relevant to Biosynthetic Research on Vitamin $B_{12}$. Part 12. Modification of the Periphery of Chlorins and Isobacteriochlorins. *J. Chem. Soc., Perkin Trans. 1* **1997**, 1105−1116.

(17) Smith, K. M.; Simpson, D. J. Raney Nickel Reductions of Chlorophyll Derivatives: Hydroporphyrins in the Anhydro Series. *J. Am. Chem. Soc.* **1987**, *109*, 6326−6333.
(18) Ide, Y.; Kuwahara, T.; Takeshita, S.; Fujishiro, R.; Suzuki, M.; Mori, S.; Shinokubo, H.; Nakamura, M.; Yoshino, K.; Ikeue, T. Nickel (II) Pyrrocorphin: Enhanced Binding Ability in a Highly Reduced Porphyrin Complex. *J. Inorg. Biochem.* **2018**, *178*, 115−124.
(19) Silva, A. M. G.; Tomé, A. C.; Neves, M. G. P. M. S.; Silva, A. M. S.; Cavaleiro, J. A. S. 1,3-Dipolar Cycloaddition Reactions of Porphyrins with Azomethine Ylides. *J. Org. Chem.* **2005**, *70*, 2306−2314.
(20) Yu, Y.; Furuyama, T.; Tang, J.; Wu, Z.-Y.; Chen, J.-Z.; Kobayashi, N.; Zhang, J.-L. Stable Iso-Bacteriochlorin Mimics from Porpholactone: Effect of a β-Oxazolone Moiety on the Frontier π-Molecular Orbitals. *Inorg. Chem. Front.* **2015**, *2*, 671−677.
(21) Peters, M. K.; Röhricht, F.; Näther, C.; Herges, R. One-Pot Approach to Chlorins, Isobacteriochlorins, Bacteriochlorins, and Pyrrocorphins. *Org. Lett.* **2018**, *20*, 7879−7883.
(22) Fischer, H.; Orth, H.: *Die Chemie des Pyrrols*; Akademische Verlagsgesellschaft (Johnson Reprint, New York 1968): Leipzig, 1937; Vol. *II*, Part I, pp 59−60.
(23) Bonnett; Dolphin, D.; Johnson, A. W.; Oldfield, D.; Stephenson, G. F. Oxidation of Porphyrins with $H_2O_2$ in $H_2SO_4$. *Proc. Chem. Soc.* **1964**, *Nov*, 371−372.
(24) Bonnett, R.; Dimsdale, M. J.; Stephenson, G. F. *meso*-Reactivity of Porphyrins and Related Compounds. IV. Introduction of Oxygen Functions. *J. Chem. Soc. C* **1969**, 564−570.
(25) Inhoffen, H. H.; Nolte, W. Zur Weiteren Kenntnis des Chlorophylls und des Hämins XV. Umwandlungen des Octaethylporphyrins in Octaethyl-Geminiporphyrin-Polyketone. *Tetrahedron Lett.* **1967**, *8*, 2185−2187.
(26) Inhoffen, H. H.; Nolte, W. Chlorophyll and Hemin. XXIV. Oxidative Rearrangements of Octaethylporphine to Geminiporphine Polyketones. *Justus Liebigs Ann. Chem.* **1969**, *725*, 167−176.
(27) Chang, C. K. Synthesis and Characterization of Alkylated Isobacteriochlorins Models of Siroheme and Sirohydrochlorin. *Biochemistry* **1980**, *19*, 1971−1976.
(28) Brückner, C.; Chaudhri, N.; Nevonen, D. E.; Bhattacharya, S.; Graf, A.; Kaesmann, E.; Li, R.; Guberman-Pfeffer, M. J.; Mani, T.; Nimthong-Roldán, A.; et al. Structural and Photophysical Characterization of All Five Constitutional Isomers of the Octaethyl-β,β′-dioxo-bacterio- and -isobacteriochlorin Series. *Chem. - Eur. J.* **2021**, *27*, 16189−16203.
(29) Chaudhri, N.; Guberman-Pfeffer, M. J.; Li, R.; Zeller, M.; Brückner, C. β-Trioxopyrrocorphins: Pyrrocorphins of Graded Aromaticity. *Chem. Sci.* **2021**, *12*, 12292−12301.
(30) Stolzenberg, A. M.; Glazer, P. A.; Foxman, B. M. Structure, Reactivity, and Electrochemistry of Free-Base β-Oxoporphyrins and Metallo-β-Oxoporphyrin. *Inorg. Chem.* **1986**, *25*, 983−991.
(31) Stolzenberg, A. M.; Stershic, M. T. Reductive Chemistry of Nickel Hydroporphyrins: The Nickel(I) Octaethylisobacteriochlorin Anion. *Inorg. Chem.* **1987**, *26*, 3082−3083.
(32) Stolzenberg, A. M.; Steshic, M. T. Reductive Chemistry of Nickel Hydroporphyrins. Evidence for a Biologically Significant Difference Porphyrins, Hydroporphyrins, and Other Tetrapyrroles. *J. Am. Chem. Soc.* **1988**, *110*, 6391−6402.
(33) Bonnett, R.; Nizhnik, A. N.; Berenbaum, M. C. Second Generation Tumor Photosensitizers: The Synthesis of Octaalkylchlorins and Bacteriochlorins with Graded Amphiphilic Character. *J. Chem. Soc., Chem. Commun.* **1989**, 1822−1823.
(34) Stolzenberg, A. M.; Simerly, S. W.; Steffey, B. D.; Haymond, G. S. The Synthesis, Properties, and Reactivities of Free-Base- and Zn(II)-*N*-Methyl Hydroporphyrin Compounds. The Unexpected Selectivity of the Direct Methylation of Free-Base Hydroporphyrin Compounds. *J. Am. Chem. Soc.* **1997**, *119*, 11843−11854.
(35) Stolzenberg, A. M.; Laliberte, M. A. Deuterium Exchange Reactions of Oxoporphyrin Compounds. *J. Org. Chem.* **1987**, *52*, 1022−1027.
(36) Adams, K. R.; Berenbaum, M. C.; Bonnett, R.; Nizhnik, A. N.; Salgado, A.; Valles, M. A. Second Generation Tumour Photosensitisers: The Synthesis and Biological Activity of Octaalkyl Chlorins and Bacteriochlorins with Graded Amphiphilic Character. *J. Chem. Soc., Perkin Trans. 1* **1992**, 1465−1470.
(37) Arasasingham, R. D.; Balch, A. L.; Olmstead, M. M. Synthesis and Structural Characterization of Octaethyl-17-Thiochlorin and Octaethyl-7,17-Dithioisobacteriochlorin. *Heterocycles* **1988**, *27*, 2111−2118.
(38) Meehan, E.; Li, R.; Zeller, M.; Brückner, C. Octaethyl-1,3-oxazinochlorin: A β-Octaethylchlorin Analogue Made by Pyrrole Expansion. *Org. Lett.* **2015**, *17*, 2210−2213.
(39) Li, R.; Meehan, E.; Zeller, M.; Brückner, C. Surprising Outcomes of Classic Ring-Expansion Conditions Applied to Octaethyloxochlorin, 2. Beckmann-Rearrangement Conditions. *Eur. J. Org. Chem.* **2017**, 1826−1834.
(40) Li, R.; Zeller, M.; Brückner, C. Surprising Outcomes of Classic Ring-Expansion Conditions Applied to Octaethyloxochlorin, 1. Baeyer−Villiger-Oxidation Conditions. *Eur. J. Org. Chem.* **2017**, 1820−1825.
(41) Li, R.; Zeller, M.; Bruhn, T.; Brückner, C. Surprising Outcomes of Classic Ring-Expansion Conditions Applied to Octaethyloxochlorin, 3. Schmidt-Reaction Conditions. *Eur. J. Org. Chem.* **2017**, 1835−1842.
(42) Cai, S.; Belikova, E.; Yatsunyk, L. A.; Stolzenberg, A. M.; Walker, F. A. Magnetic Resonance and Structural Investigations of (Monooxooctaethylchlorinato)Iron(III) Chloride and its Bis-(Imidazole) Complex. *Inorg. Chem.* **2005**, *44*, 1882−1889.
(43) Papkovsky, D. B.; Ponomarev, G. V.; Trettnak, W.; O'Leary, P. Phosphorescent Complexes of Porphyrin Ketones: Optical Properties and Application to Oxygen Sensing. *Anal. Chem.* **1995**, *67*, 4112−4117.
(44) Neal, T. J.; Kang, S.-J.; Schulz, C. E.; Scheidt, W. R. Molecular Structures and Magnetochemistry of Two (β-Oxooctaethylchlorinato)Copper(II) Derivatives: [Cu(OxoECC)] and [Cu(OxoOEC·)]$SbCl_6$. *Inorg. Chem.* **1999**, *38*, 4294−4302.
(45) Tutunea, F.; Ryan, M. D. Visible and Infrared Spectroelectrochemistry of Cobalt Porphinones and Porphinediones. *J. Electroanal. Chem.* **2012**, *670*, 16−22.
(46) Neal, T. J.; Kang, S.-J.; Turowska-Tyrk, I.; Schulz, C. E.; Scheidt, W. R. Magnetic Interactions in the High-Spin Iron(III) Oxooctaethylchlorinato Derivative [Fe(OxoOEC)(Cl)] and Its π-Cation Radical [Fe(OxoOEC·)(Cl)]$SbCl_6$. *Inorg. Chem.* **2000**, *39*, 872−880.
(47) Chaudhri, N.; Guberman-Pfeffer, M. J.; Zeller, M.; Brückner, C. Stepwise Reduction of β-Trioxopyrrocorphins: Collapse of the Oxo-Induced Macrocycle Aromaticity. *J. Org. Chem.* **2022**, *87*, 7179−7192.
(48) Connick, P. A.; Macor, K. A. Spectroscopic and Electrochemical Characterization of Nickel β-Oxoporphyrins: Identification of Nickel(III) Oxidation Products. *Inorg. Chem.* **1991**, *30*, 4654−4663.
(49) Connick, P. A.; Haller, K. J.; Macor, K. A. X-Ray Structural and Imidazole-Binding Studies of Nickel β-Oxoporphyrins. *Inorg. Chem.* **1993**, *32*, 3256−3264.
(50) Chang, C. K.; Barkigia, K. M.; Hanson, L. K.; Fajer, J. Models of Heme d1. Structure and Redox Chemistry of Dioxoisobacteriochlorins. *J. Am. Chem. Soc.* **1986**, *108*, 1352−1354.
(51) Barkigia, K. M.; Chang, C. K.; Fajer, J.; Renner, M. W. Models of Heme d1. Molecular Structure and NMR Characterization of an Iron(III) Dioxoisobacteriochlorin (Porphyrindione). *J. Am. Chem. Soc.* **1992**, *114*, 1701−1707.
(52) Ozawa, S.; Sakamoto, E.; Watanabe, Y.; Morishima, I. Formation of Nitrosyl-Iron(II)-β-Oxoporphyrin π-Cation Radical Complexes. Models for a Reaction Intermediate of Dissimilatory Nitrite Reductases. *J. Chem. Soc., Chem. Commun.* **1994**, 935−936.
(53) Schnable, D.; Chaudhri, N.; Li, R.; Zeller, M.; Brückner, C. Evaluation of Octaethyl-7,17-dioxobacteriochlorin as a Ligand for Transition Metals. *Inorg. Chem.* **2020**, *59*, 2870−2880.


https://doi.org/10.1021/acs.jpca.3c03184
J. Phys. Chem. A 2023, 127, 7694−7706

(54) Fujii, H.; Yamaki, D.; Ogurac, T.; Hadab, M. The Functional Role of the Structure of the Dioxoisobacteriochlorin in the Catalytic Site of Cytochrome cd1 for the Reduction of Nitrite. *Chem. Sci.* **2016**, *7*, 2896−2906.
(55) Chaudhri, N.; Zeller, M.; Brückner, C. Stepwise Reduction of Octaethyl-$\beta,\beta'$-dioxochlorin Isomers: Access to Structurally and Electronically Diverse Hydroporphyrins. *J. Org. Chem.* **2020**, *85*, 13951−13964.
(56) Bhattacharya, S.; Graf, A.; Gomes, A. K. M. S.; Chaudhri, N.; Chekulaev, D.; Brückner, C.; Cardozo, T. M.; Chauvet, A. A. P. Tailoring the Intersystem Crossing and Triplet Dynamics of Free-Base Octaalkyl-$\beta$-oxo-Substituted Porphyrins: Competing Effects of Spin−Vibronic and NH Tautomerism Relaxation Channels. *J. Phys. Chem. A* **2022**, *126*, 2522−2531.
(57) Ke, X.-S.; Chang, Y.; Chen, J.-Z.; Tian, J.; Mack, J.; Cheng, X.; Shen, Z.; Zhang, J.-L. Porphodilactones as Synthetic Chlorophylls: Relative Orientation of $\beta$-Substituents on a Pyrrolic Ring Tunes NIR Absorption. *J. Am. Chem. Soc.* **2014**, *136*, 9598−9607.
(58) Ning, Y.; Jin, G.-Q.; Zhang, J.-L. Porpholactone Chemistry: An Emerging Approach to Bioinspired Photosensitizers with Tunable Near-Infrared Photophysical Properties. *Acc. Chem. Res.* **2019**, *52*, 2620−2633.
(59) Ning, Y.; Liu, Y. W.; Yang, Z. S.; Yao, Y.; Kang, L.; Sessler, J. L.; Zhang, J. L. Split and Use: Structural Isomers for Diagnosis and Therapy. *J. Am. Chem. Soc.* **2020**, *142*, 6761−6768.
(60) Hewage, N.; Daddario, P.; Lau, K. S. F.; Guberman-Pfeffer, M. J.; Gascón, J. A.; Zeller, M.; Lee, C. O.; Khalil, G. E.; Gouterman, M.; Brückner, C. Bacterio- and Isobacteriodilactones by Stepwise or Direct Oxidations of *meso*-Tetrakis(pentafluorophenyl)-porphyrin. *J. Org. Chem.* **2019**, *84*, 239−256.
(61) Connick, P. A. Electrochemical Titrations of Nickel $\beta$-Oxoporphyrins with Imidazole. *Electrochem. Soc. Interface* **1993**, *2*, 51−52.
(62) Tyrk, T.; Kang, I.; Joo, S.; Scheidt, W. R. Conformational Distortions of $\pi$-Cation Radical ($\beta$-Oxoporphyrin)Copper(II) Derivatives: [Cu(2,7,12-TrioxoOEHP)][$SbCl_6$] and [Cu(2,7-DioxoOEiBC·)][$SbCl_6$]. *J. Porphyrins Phthalocyanines* **2011**, *15*, 373−381.
(63) Taniguchi, M.; Lindsey, J. S.; Bocian, D. F.; Holten, D. Comprehensive Review of Photophysical Parameters ($\varepsilon$, Φf, $\tau$s) of Tetraphenylporphyrin ($H_2$TPP) and Zinc Tetraphenylporphyrin (ZnTPP) − Critical Benchmark Molecules in Photochemistry and Photosynthesis. *J. Photochem. Photobiol., C* **2021**, *46*, No. 100401.
(64) Schmidt, R.; Tanielian, C.; Dunsbach, R.; Wolff, C. Phenalenone, a Universal Reference Compound for the Determination of Quantum Yields of Singlet Oxygen $O_2(^1\Delta_g)$ Sensitization. *J. Photochem. Photobiol., A* **1994**, *79*, 11−17.
(65) Mason, W. R.: *A Practical Guide to Magnetic Circular Dichroism Spectroscopy*; John Wiley & Sons, Inc: Hoboken, NJ, 2007, pp 1−223.
(66) Mack, J.; Kobayashi, N. Low Symmetry Phthalocyanines and Their Analogues. *Chem. Rev.* **2011**, *111*, 281−321.
(67) Kobayashi, N.; Muranaka, A.; Mack, J.: *Circular Dichroism and Magnetic Circular Dichroism Spectroscopy for Organic Chemists*; RSC: London, 2011, pp 1−216.
(68) Frisch, M. J.; Trucks, G. W.; Schlegel, H. B.; Scuseria, G. E.; Robb, M. A.; Cheeseman, J. R.; Scalmani, G.; Barone, V.; Mennucci, B.; Petersson, G. A.; et al. *Gaussian 09*; Gaussian, Inc.: Wallingford, CT, USA, 2009.
(69) Yanai, T.; Tew, D. P.; Handy, N. C. A New Hybrid Exchange−Correlation Functional Using the Coulomb-Attenuating Method (CAM-B3LYP). *Chem. Phys. Lett.* **2004**, *393*, 51−57.
(70) Zhao, Y.; Truhlar, D. G. The M06 Suite of Density Functionals for Main Group Thermochemistry, Thermochemical Kinetics, Noncovalent Interactions, Excited States, and Transition Elements: Two New Functionals and Systematic Testing of Four M06-Class Functionals and 12 Other Functionals. *Theor. Chem. Acc.* **2008**, *120*, 215−241.
(71) Tomasi, J.; Mennucci, B.; Cammi, R Quantum Mechanical Continuum Solvation Models. *Chem. Rev.* **2005**, *105*, 2999−3094.
(72) McLean, A. D.; Chandler, G. S. Contracted Gaussian-Basis Sets for Molecular Calculations. 1. 2nd Row Atoms, Z=11-18. *J. Chem. Phys.* **1980**, *72*, 5639−5648.
(73) Tenderholt, A. L. *QMForge*, 2.1 ed.; Stanford University: Stanford, CA, 2011.
(74) Yao, Y.; Rao, Y.; Liu, Y.; Jiang, L.; Xiong, J.; Fan, Y. J.; Shen, Z.; Sessler, J. L.; Zhang, J. L. Aromaticity Versus Regioisomeric Effect of $\beta$-Substituents in Porphyrinoids. *Phys. Chem. Chem. Phys.* **2019**, *21*, 10152−10162.
(75) Baskin, J. S.; Yu, H.-Z.; Zewail, A. H. Ultrafast Dynamics of Porphyrins in the Condensed Phase: I. Free Base Tetraphenylporphyrin. *J. Phys. Chem. A* **2002**, *106*, 9837−9844.
(76) Chirvony, V. S.; van Hoek, A.; Galievsky, V. A.; Sazanovich, I. V.; Schaafsma, T. J.; Holten, D. Comparative Study of the Photophysical Properties of Nonplanar Tetraphenylporphyrin and Octaethylporphyrin Diacids. *J. Phys. Chem. B* **2000**, *104*, 9909−9917.
(77) Ziegler, C. J.; Sabin, J. R.; Geier, G. R.; Nemykin, V. N. The first TDDFT and MCD Studies of Free Base Triarylcorroles: A Closer Look into Solvent-dependent UV-visible Absorption. *Chem. Commun.* **2012**, *48*, 4743−4745.
(78) Rhoda, H. M.; Akhigbe, J.; Ogikubo, J.; Sabin, J. R.; Ziegler, C. J.; Brückner, C.; Nemykin, V. N. Magnetic Circular Dichroism Spectroscopy of *meso*-Tetraphenylporphyrin-Derived Hydroporphyrins and Pyrrole-Modified Porphyrins. *J. Phys. Chem. A* **2016**, *120*, 5805−5815.
(79) Doble, S.; Osinski, A. J.; Holland, S. M.; Fisher, J. M.; Geier, G. R.; Belosludov, R. V.; Ziegler, C. J.; Nemykin, V. N. Magnetic Circular Dichroism of Transition-Metal Complexes of Perfluorophenyl-N-Confused Porphyrins: Inverting Electronic Structure through a Proton. *J. Phys. Chem. A* **2017**, *121*, 3689−3698.
(80) Ziegler, C. J.; Erickson, N. R.; Dahlby, M. R.; Nemykin, V. N. Magnetic Circular Dichroism Spectroscopy of N-Confused Porphyrin and Its Ionized Forms. *J. Phys. Chem. A* **2013**, *117*, 11499−11508.
(81) Mack, J.; Stone, J.; Nyokong, T. Trends in the TD-DFT calculations of Porphyrin and Phthalocyanine Analogs. *J. Porphyrins Phthalocyanines* **2014**, *18*, 630−641.
(82) Mack, J. Expanded, Contracted, and Isomeric Porphyrins: Theoretical Aspects. *Chem. Rev.* **2017**, *117*, 3444−3478.
(83) Gorski, A.; Kijak, M.; Zenkevich, E.; Knyukshto, V.; Starukhin, A.; Semeikin, A.; Lyubimova, T.; Roliński, T.; Waluk, J. Magnetic Circular Dichroism of *meso*-Phenyl-Substituted Pd-Octaethylporphyrins. *J. Phys. Chem. A* **2020**, *124*, 8144−8158.
(84) Kowalska, P.; Gawinkowski, S.; Sarma, T.; Panda, P. K.; Waluk, J. Structure, Electronic States, and Anion-Binding Properties of Cyclo[4]Naphthobipyrroles. *J. Phys. Chem. A* **2014**, *118*, 1038−1046.
(85) Waluk, J.; Müller, M.; Swiderek, P.; Kocher, M.; Vogel, E.; Hohlneicher, G.; Michl, J. Electronic States of Porphycenes. *J. Am. Chem. Soc.* **1991**, *113*, 5511−5527.
(86) Waluk, J.; Hemmi, G.; Sessler, J. L.; Michl, J. Magnetic Circular Dichroism of Metallotexaphyrins. *J. Org. Chem.* **1991**, *56*, 2735−2742.
(87) Wee, A. G. H.; Shu, A. Y. L.; Bunnenberg, E.; Djerassi, C. Magnetic Circular Dichroism Studies. 66. Synthesis of Demethyl Monosubstituted Porphyrins. The Effect of Substituent Conformation on the Magnetic Circular Dichroism Spectra of Ethoxycarbonyl Porphyrins. *J. Org. Chem.* **1984**, *49*, 3327−3336.
(88) Goldbeck, R. A. Sign Variation in the Magnetic Circular Dichroism Spectra of P-Substituted Porphyrins. *Acc. Chem. Res.* **1988**, *21*, 95−101.
(89) Gouterman, M. Spectra of Porphyrins. *J. Mol. Spectrosc.* **1961**, *6*, 138−163.
(90) Zenkevich; Shulga, A. M.; Chernook, A. V.; Filatov, I. V.; Gurinovich, G. P. *Teor. Eksp. Khim.* **1989**, *25*, 295−305.


https://doi.org/10.1021/acs.jpca.3c03184
J. Phys. Chem. A 2023, 127, 7694−7706

(91) Ishizuka, T.; Sakashita, R.; Iwanaga, O.; Morimoto, T.; Mori, S.; Ishida, M.; Toganoh, M.; Takegoshi, K.; Osuka, A.; Furuta, H. NH Tautomerism of N-Confused Porphyrin: Solvent/Substituent Effects and Isomerization Mechanism. *J. Phys. Chem. A* **2020**, *124*, 5756−5769.
(92) Umetani, M.; Kim, G.; Tanaka, T.; Kim, D.; Osuka, A. Rational Synthesis of 5,10-Diazaporphyrins via Nucleophilic Substitution Reactions of $\alpha,\alpha'$-Dibromotripyrrin and Dihydrogenation to Give 5,10-Diazachlorins. *J. Org. Chem.* **2020**, *85*, 3849−3857.
(93) Taniguchi, M.; Mass, O.; Boyle, P. D.; Tang, Q.; Diers, J. R.; Bocian, D. F.; Holten, D.; Lindsey, J. S. Structural Studies of Sparsely Substituted Synthetic Chlorins and Phorbines Establish Benchmarks for Changes in the Ligand Core and Framework of Chlorophyll Macrocycles. *J. Mol. Struct.* **2010**, *979*, 27−45.
(94) Wacker, P.; Dahms, K.; Senge, M. O.; Kleinpeter, E. Influence of the Core Conformation on the NH-Tautomerism in Porphyrins: A Study of *meso*-(1,3-Dithian-2-yl)porphyrins. *J. Org. Chem.* **2008**, *73*, 2182−2190.
(95) Punnagai, M.; Sateesh, B.; Sastry, G. N. A Density Functional Theory Study on the Porphyrin Isomers: Effect of *meso*-Bridge Length, Relative Stabilities, *cis-trans*-Isomerism. *ARKIVOC* **2005**, 258−283.
(96) Furuta, H.; Maeda, H.; Osuka, A. Theoretical Study of Stability, Structures, and Aromaticity of Multiply N-Confused Porphyrins. *J. Org. Chem.* **2001**, *66*, 8563−8572.
(97) Nemykin, V. N.; Sabin, J. R. Profiling Energetics and Spectroscopic Signatures in Prototropic Tautomers of Asymmetric Phthalocyanine Analogues. *J. Phys. Chem. A* **2012**, *116*, 7364−7371.
(98) Turro, N. J.; Ramamurthy, V.; Scaiano, J. C.: *Modern Molecular Photochemistry of Organic Molecules*; University Science Books: California, 2010.
(99) Jeong, H.-G.; Choi, M.-S. Design and Properties of Porphyrin-based Singlet Oxygen Generator. *Isr. J. Chem.* **2016**, *56*, 110−118.
(100) Zapata, F.; Nucci, M.; Castaño, O.; Marazzi, M.; Frutos, L. M. Thermal and Mechanochemical Tuning of the Porphyrin Singlet-Triplet Gap for Selective Energy Transfer Processes: A Molecular Dynamics Approach. *J. Chem. Theory Comput.* **2021**, *17*, 5429−5439.
(101) Oh, J.; Sung, Y. M.; Hong, Y.; Kim, D. Spectroscopic Diagnosis of Excited-State Aromaticity: Capturing Electronic Structures and Conformations upon Aromaticity Reversal. *Acc. Chem. Res.* **2018**, *51*, 1349−1358.
(102) Ueta, K.; Kim, J.; Ooi, S.; Oh, J.; Shin, J.; Nakai, A.; Lim, M.; Tanaka, T.; Kim, D.; Osuka, A. *meso*-Oxoisocorroles: Tunable Antiaromaticity by Metalation and Coordination of Lewis Acids as Well as Aromaticity Reversal in the Triplet Excited State. *J. Am. Chem. Soc.* **2021**, *143*, 7958−7967.
(103) Hewage, N.; Guberman-Pfeffer, M. J.; Chaudhri, N.; Zeller, M.; Gascón, J. A.; Brückner, C. Syntheses and Aromaticity Parameters of Hexahydroxypyrrocorphin, Porphotrilactones, and Their Oxidation State Intermediates. *J. Org. Chem.* **2022**, *87*, 12096−12108.


https://doi.org/10.1021/acs.jpca.3c03184
*J. Phys. Chem. A* 2023, 127, 7694−7706